Characterization of GPS time series at the Neapolitan volcanic area by statistical analysis

M. Bottiglieri,[1] M. Falanga,[2] U. Tammaro,[3] P. De Martino,[3] F. Obrizzo,[3] C. Godano,[1] and F. Pingue[3]

Received 6 May 2009; revised 12 February 2010; accepted 2 March 2010; published 21 October 2010.

[1] The GPS time series recorded at the Neapolitan volcanic area reveals a very peculiar behavior. When a clear deformation is observed, the amplitude distribution evolves from a super-Gaussian to a broader distribution. This behavior can be characterized by evaluating the kurtosis. Spurious periodic components were evidenced by independent component analysis and then removed by filtering the original signal. The time series for all stations was modeled with a fifth-order polynomial fit, which represents the deformation history at that place. Indeed, when this polynomial is subtracted from the time series, the distributions again become super-Gaussian. A simulation of the deformation time evolution was performed by superposing a Laplacian noise and a synthetic deformation history. The kurtosis of the obtained signals decreases as the superposition increases, enlightening the insurgence of the deformation. The presented approach represents a contribution aimed at adding further information to the studies about the deformation at the Neapolitan volcanic area by revealing geologically relevant data.

Citation: Bottiglieri, M., M. Falanga, U. Tammaro, P. De Martino, F. Obrizzo, C. Godano, and F. Pingue (2010), Characterization of GPS time series at the Neapolitan volcanic area by statistical analysis, *J. Geophys. Res.*, *115*, B10416, doi:10.1029/2009JB006594.

1. Introduction

[2] The correct definition of the background level of ground deformation is a very important aspect in geodetic monitoring of volcanic areas. Indeed, it could allow a fast identification of an anomalous deformation trend that evolves toward an eruptive event. The definition of the noise level is necessary to identify transient deformations owing to stress modifications in the upper crust, such as tectonic processes and fault slipping. Furthermore, in volcanic areas these deformations can be generated by the movement or pressure changes of magmatic masses. Then, the noise level definition becomes crucial in assessing volcanic hazard.

[3] In fact, the GPS time series can be considered the superposition of many effects owing to several origins such as tides, ionosphere, and troposphere; other sources of deformations can be ascribed to stress modifications in Earth's crust [*Beran*, 1994; *van Dam et al.*, 1994; *Langbein and Johnson*, 1997; *Mao et al.*, 1999; *Dong et al.*, 2002; *Williams*, 2003; *Williams et al.*, 2004; *Watson et al.*, 2006].

[4] The known source effects are usually removed by means of standard analysis procedures [*Dach et al.*, 2007]. Nevertheless, preprocessed data can be affected by significant residuals, including site effects and noise. These contributions can be considered to constitute the background level, whereas any other measurable deformation could represent the source-driven ground movements.

[5] In the present paper, we show that any ground deformation modifies the distribution of the time-series amplitude so significantly that it can be used as the marker of an effective source-driven deformation. In the following, we present an approach to evidence in the background of the insurgence of a ground deformation, whose amount can be quantified by the kurtosis. The latter is a good estimator of non-Gaussian processes.

[6] We analyze the site position time series of the Neapolitan Volcanic Continuous GPS (NeVoCGPS) network, operating on three volcanic active districts: Somma-Vesuvius volcano, Campi Flegrei caldera, and Ischia Island. The concentration of these active volcanoes in an area with dense urbanization needs systematic monitoring to collect data to characterize eruptive precursors that are useful for modeling the volcanoes' behavior.

2. Data Set

[7] We focus our attention on the ground deformation acquired by a dense GPS network in the Napolitan volcanic area (southern Italy), indicated in Figure 1.

2.1. Geological Setting

[8] The Neapolitan volcanic area occupies part of the South Campania plain, a tectonic depression delimited by carbo-

[1]Dipartimento di Scienze Ambientali, Seconda Università degli Studi di Napoli, Caserta, Italy.
[2]Dipartimento di Matematica e Informatica, Università di Salerno, Fisciano (SA), Italy.
[3]Istituto Nazionale di Geofisica e Vulcanologia, Osservatorio Vesuviano, Naples, Italy.

0148-0227/10/2009JB006594

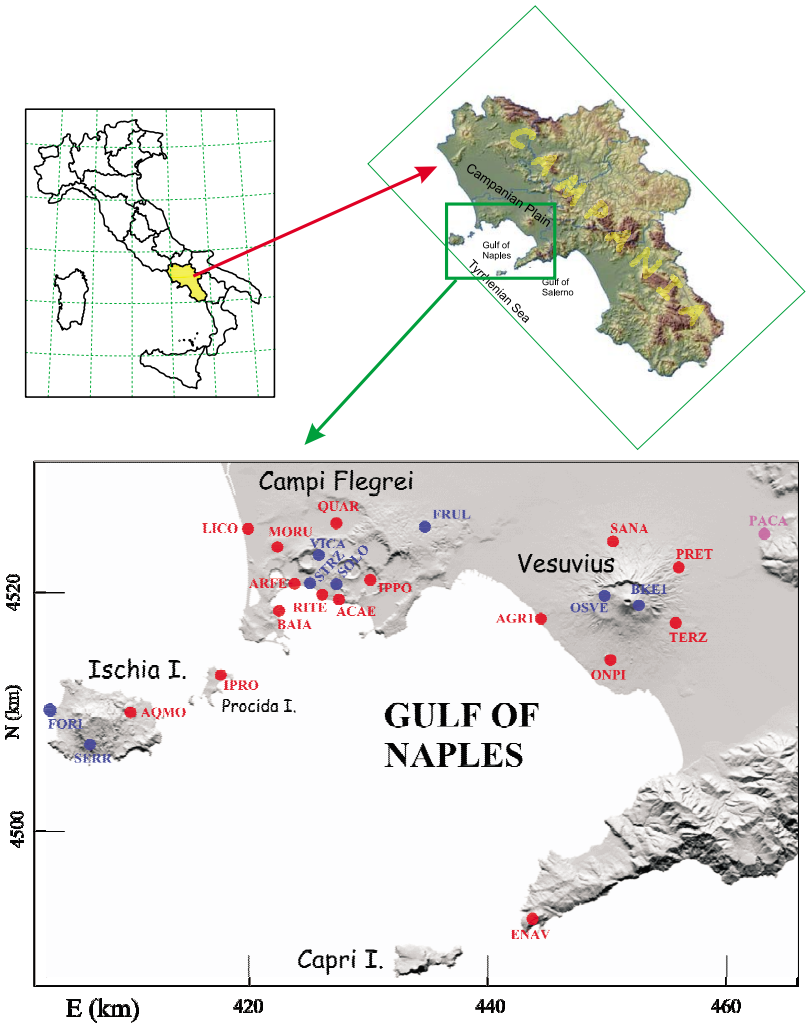

Figure 1. Map of the NeVoCGPS network: red circles indicate the stations used in the present analysis, blue circles represent the abolished stations; the reference station is PACA.

natic platforms and by the Tyrrhenian Sea (Figure 1). The opening of the Tyrrhenian Sea and the anticlockwise rotation of the Italian peninsula has caused stretching and thinning of the mantle in the western edge, with the development of intense volcanic activity [*Scandone*, 1979; *Judenherc and Zollo*, 2004; *Patacca and Scandone*, 2007]. The Vesuvius volcano, situated east of Naples is quiescent (the last eruption occurred in 1944). It is characterized by low-level seismicity and deformation activity [*De Natale et al.*, 2006]. Campi Flegrei (the last eruption occurred in 1538) are characterized by a slow deformation called bradyseism. During the periods 1969–1972 and 1982–1984, the Campi Flegrei caldera was affected by two intense episodes of ground uplift. In 1985, a subsidence phase started, with episodic miniuplifts superimposed [*Troise et al.*, 2008; *Gaeta et al.*, 2003; *Battaglia et al.*, 2006]. Ischia Island has been characterized by both explosive and effusive eruptive activity (the last occurred in 1302). Successively, dynamics have been characterized by seismic activity (where the strongest events occurred in 1881 and 1883) and by meaningful subsidence in the southern and northwestern sectors of the island [*Carlino et al.*, 2006].

2.2. NeVoCGPS Network

[9] The NeVoCGPS network consists of 25 stations (shown in Figure 1) with a configuration that guarantees constant and fast 3-D information about the dynamics of the Neapolitan volcanic area. This network is part of the Neapolitan volcanoes geodetic monitoring system operating at the INGV-Osservatorio Vesuviano.

[10] All the stations are managed by remote control and the data are automatically downloaded and processed on a daily basis using the Ultra-rapid International GNSS Service (IGS) products [*Dow et al.*, 2009]. When the IGS final orbits and Earth rotation parameters (ERPs) become available, the data are reprocessed. The data processing is performed by the Bernese Processing Engine of the Bernese GPS software version 5.0 [*Dach et al.*, 2007] in double difference mode. The elevation cutoff is set at 15° and the IGS absolute phase center variations (APCVs) for the satellite and receiver antennas are applied [*Schmid et al.*, 2007]. To maximize the number of observations, independent baselines are created using the OBSMAX strategy and the ambiguity resolution is performed using the Quasi Ionosphere Free (QIF) method.

The daily station coordinates are estimated, together with the troposphere, in the final ionospheric free L3 solution. The troposphere is modeled using the dry-Niell a priori model and estimating the Tropospheric Zenith Delay (TZD) parameters each hour at each site using the wet-Niell mapping function. The datum definition is realized by three no-net-translation conditions (minimal constraint) imposed on a set of six IGS05 fiducial sites [*Ferland*, 2006], which are included in the processing.

[11] To get homogeneous results, all the GPS data collected before the introduction of the new realization of the International Terrestrial Reference System (IGS05) in November 2006 were reprocessed using the orbits and ERPs obtained by the GPS reprocessing project GPS-PDR [*Steigenberger et al.*, 2006]. These products are in the IGb00 reference system [*Ray et al.*, 2004] and they are estimated by applying the APCVs.

[12] To minimize the contribution of tectonic movements, the GPS position time series are estimated relative to the stable station PACA located outside the volcanic area.

[13] In our analysis, we used the data recorded during the period 2001–2007 [*De Martino et al.*, 2007]. We selected those stations that provided the best quality GPS time series and that worked for the longest period (about 4 years). Namely, we excluded the stations identified by blue circles in Figure 1 (BKE1, FORI, FRUL, OSVE, SERR, SOLO, STRZ, and VICA) because the recorded time series were too short or exhibited prolonged bad data. Hence, we focused our attention on the daily measurements of the three components of the ground deformation recorded at 16 stations shown as red circles in Figure 1.

3. Data Analysis

[14] The complexity of the phenomena that occur in the investigated area leads us to assume a time domain approach. Namely, this domain is suitable to extract information from nonlinear data such as GPS time series, which are still affected by residual signals, though they are preprocessed as indicated in the section 2.2. To investigate the presence of the residual effects, we decided to apply independent component analysis (ICA), which is a nonlinear technique operating in the time domain and based on high-order statistics.

3.1. Independent Component Analysis Technique

[15] ICA is a method to find underlying factors or components from multivariate statistical data [see, e.g., *Hyvärinen et al.*, 2001]. It is very closely related to the method called blind source separation (BSS). One of the main goals in BSS is the extraction of independent sources from their linear mixtures. To explain the problem, we consider some signals emitted by different physical sources: we assume that there are some sensors and that they are in different positions so that each sensor records a mixture of the source signals with different weights. In this case, we use an instantaneous mixing model, where we neglect any time delays that may occur in the mixing. Formally, the mixing model is written as

$$\mathbf{x} = \mathbf{A}\mathbf{s} + \mathbf{n}, \tag{1}$$

where $\mathbf{x}$ is an observed m-D vector, $\mathbf{s}$ is an n-D random vector whose components are assumed to be mutually independent, $\mathbf{A}$ is a constant $m \times n$ matrix to be estimated, and $\mathbf{n}$ is the additive noise. The additive noise term $\mathbf{n}$ is often omitted in previous studies because it can be incorporated in the sum as one of the source signals. In addition to the independent assumption among components, we assume that the number of available different mixtures, m, is at least as large as the number of sources, n. Usually, m is assumed to be known in advance, and often $m = n$. Only one of the source signals, s_i, is allowed to have a Gaussian distribution, because it is impossible to separate two or more Gaussian sources [*Bell and Sejnowski*, 1995; *Karhunen*, 1996]. In adaptive source separation, an $m \times n$ separating matrix $\mathbf{B}$ is updated so that the vector $\mathbf{y} = \mathbf{B}\mathbf{x}$ is an estimate $\mathbf{y} \cong \mathbf{s}$ of the original independent source signals. In the following, we use the fixed-point algorithm, namely FastICA [*Hyvärinen et al.*, 2001]. The FastICA learning rule finds a direction, that is, a unit vector $\mathbf{w}$ such that the projection $\mathbf{w}^T\mathbf{x}$ maximizes the independence of the single estimated source y. Independence is generally measured by means of the negentropy $J(\mathbf{x}) = H(\mathbf{x}_{\text{Gauss}}) - H(\mathbf{x})$, where H is the Kolmogorov entropy defined as $H(\mathbf{x}) = -\int p_x \log p_x \, dx$ and the subscript Gauss indicates that the quantity is referred at a variable with Gaussian distribution. In the FastICA algorithm, we use an approximation of the negentropy given by

$$J_G(\mathbf{w}) = \left[E\{G(\mathbf{w}^T\mathbf{x})\} - E\{G(\nu)\}\right]^2, \tag{2}$$

where $\mathbf{w}$ is an m-D (weight) vector, $\mathbf{x}$ represents our mixture of signals, $E\{(\mathbf{w}^T\mathbf{x})^2\} = 1$, ν is a standardized Gaussian random variable, and $G(\,)$ is a suitable nonlinearity, in our case $G(y) = \log\cosh(y)$. Maximizing J_G allows us to find one independent component or projection pursuit direction. The algorithm requires a preliminary whitening of the data: the observed variable $\mathbf{x}$ is linearly transformed to a zero-mean variable $\mathbf{v} = \mathbf{Q}\mathbf{x}$ such that $E\{\mathbf{v}\mathbf{v}^T\} = I$. Whitening can always be accomplished by, for example, principal component analysis [*Hyvärinen et al.*, 2001]. The one-unit fixed-point algorithm for finding a row vector $\mathbf{w}$ is [*Hyvärinen et al.*, 2001]

$$\begin{aligned} \mathbf{w}^* &= E[\mathbf{v}g(\mathbf{w}_i^T\mathbf{v})] - E[g'(\mathbf{w}_i^T\mathbf{v})]\mathbf{w}_i, \\ \mathbf{w}_i &= \mathbf{w}_i^* / \|\mathbf{w}_i\|, \end{aligned} \tag{3}$$

where $g'(\,)$ is the derivative of $g(\,)$ [in our case, $g(y) = \tanh(y)$], and $g'(y)$ is its derivative with respect to y. The algorithm of the previous equations estimates just one of the independent components. To estimate several independent components, we need to run the one-unit FastICA algorithm using several units (e.g., neurons) with weight vectors $\mathbf{w}_1,\ldots,\mathbf{w}_n$. To prevent different vectors from converging to the same maximum, we must decorrelate the outputs $\mathbf{w}_1^T\mathbf{x},\ldots,\mathbf{w}_n^T\mathbf{x}$ after every iteration. In specific applications it may be desired to use a symmetric decorrelation, in which vectors are not privileged over the others. This can be accomplished by the classical method involving matrix square roots. The iterative procedure is started with a random (0/1) value for each weight and stopped when the differences between the weights of two successive iterations are smaller than a given threshold. If we assume that the data are whitened, we have that

$$\mathbf{W} = \mathbf{W}(\mathbf{W}^{*T}\mathbf{W}^*)^{-1/2}, \tag{4}$$

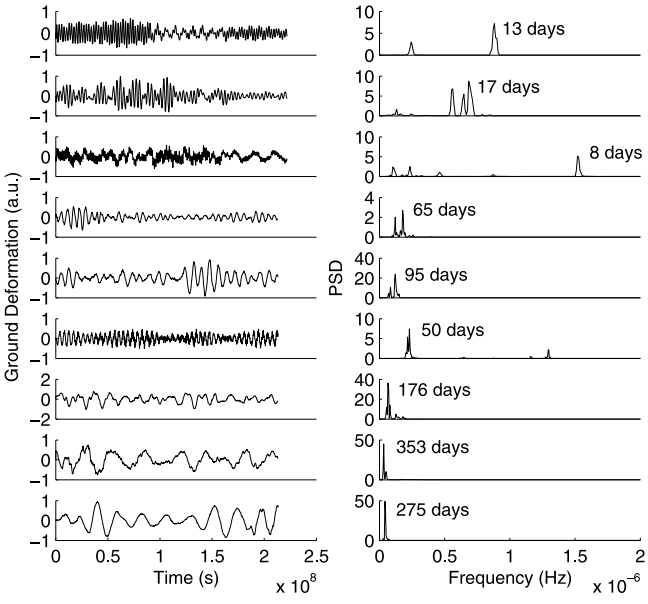

Figure 2. (left) Independent components and (right) their spectra.

where $\mathbf{W}$ is the matrix of the vectors ($\mathbf{w}_1,\ldots,\mathbf{w}_n$), and the inverse square root is obtained from the eigenvalue decomposition as

$$(\mathbf{W}^T\mathbf{W})^{-1/2} = \mathbf{E}\mathbf{D}^{-1/2}\mathbf{E}^T, \tag{5}$$

where $\mathbf{E}$ is the eigenvector matrix and $\mathbf{D}$ is the diagonal eigenvalue matrix.

3.2. Identification of Independent Components and Statistical Analysis

[16] Following the work of *Bottiglieri et al.* [2007], we considered the GPS ground deformations as mixtures of the same source signals with different weights. Therefore, we applied ICA to all the components at the selected 16 stations. ICA was able to recognize nine periodicities in the recorded signals, namely 353, 275, 176, 95, 65, 50, 17, 13, and 8 days (see Figure 2). This result is in good agreement with the previous one obtained by *Bottiglieri et al.* [2007]. Some of these periods can be connected to a physical loading effect, whereas the origins of the other periods are still uncertain [*Dong et al.*, 2002]. In particular, atmospheric load owing to pressure variations and oceanic loading exhibit annual periodicity, although both present also semiannual and ~10 day periodicity owing to weather cycles (see, among others, *Mangiarotti et al.* [2001]).

[17] A good detection of the background deformation level requires the complete absence of any of these effects. To remove them, we applied a stop-band filter for each recognized frequency as extracted by ICA. As a stop-band filter we adopted a Butterworth filter at third order. It is characterized by a magnitude response that is maximally flat in the stop band and monotonic overall; the filter sacrifices rolloff steepness for monotonicity in the stop bands. An example of the original and filtered signals is shown in Figure 3 for station ENAV.

[18] To investigate the behavior of the GPS time series, we evaluate the amplitude distribution of the signals before and after stop-band filtering. A qualitative inspection of the plots reveals that several stations exhibit a Gaussian-like shape for all three components (Figures 4 and 5), whereas in some cases the distribution appears to be broader or bimodal (Figures 6 and 7). It appears clear that no significant differences can be appreciated between the original and filtered signal distributions. The same behavior is observed for the other three stations not reported in the figures: ENAV, IPPO, and QUAR. Nevertheless, some stations exhibit a very clear difference when the original signals are filtered (see Figures 8 and 9). Indeed, some of the distributions change from being broad to being more peaked. Only the MORU station exhibits an inverse behavior; namely, two components change from peaked to broader distributions. Indeed, even if we expect that removing some noise causes the distribution to become more regular, it is very strange to observe the inverse.

[19] We remark that ICA evidences the independent signals in terms of mean field among all the investigated stations and provides, in any case, a linear decomposition of eventually nonlinear signals. This means that the contribution of each component can be different at each station. On this basis, we can hypothesize that the atypical behavior of the MORU station can be ascribed to a basically nonlinear coupling among all the periodicities identified by ICA, whose removal (in the sense of a subtraction) induces a major complexity in the recorded deformation signal.

[20] In spite of the Gaussian-like appearance of the distribution in Figures 4, 5, and 9, not one of those distributions can be considered Gaussian at a confidence level of 95%, as revealed by a standard chi-square test. Obviously, the distributions in Figures 6–8 also cannot be considered Gaussian with the same confidence level. For a better identification of the distributions, we decided to use a simple parametric test to evaluate their normalized kurtosis:

$$\kappa = \frac{\langle x^4\rangle}{(\langle x^2\rangle)^2} - 3. \tag{6}$$

[21] The parameter κ assumes characteristic values in three different cases: (1) $\kappa < 0$ for platykurtic, sub-Gaussian, or multimodal distributions; (2)$\kappa > 0$ for super-Gaussian distributions (leptokurtic); and (3) $\kappa = 0$ when the distributions are mesokurtic (the Gaussian one is the most commonly observed among them) [*Hyvärinen et al.*, 2001].

[22] In Table 1, we report the values of κ for all the stations before (top row) and after filtering (bottom row). As can be seen, the Gaussian-like distributions of Figures 4, 5, and 9 have to be viewed as super-Gaussian ($\kappa > 0$), whereas all the other shown in Figures 6 and 7 are sub-Gaussian ($\kappa < 0$) and characterized by a bimodal behavior. In all cases, we can correlate the bimodal shape of the amplitude distribution with the nonzero ground deformation. Indeed, the monomodal behavior (super-Gaussian) corresponds to no significant ground movements and is observed for all the stations in external (ENAV and LICO), insular (IPRO and AQMO) and vesuvian (SANA, TERZ, PRET, AGR1, and ONPI) areas, in agreement with previous studies [*De Natale et al.*, 2001, 2006]. Conversely, in the Campi Flegrei area, the various GPS time series (Figure 10) exhibit significant

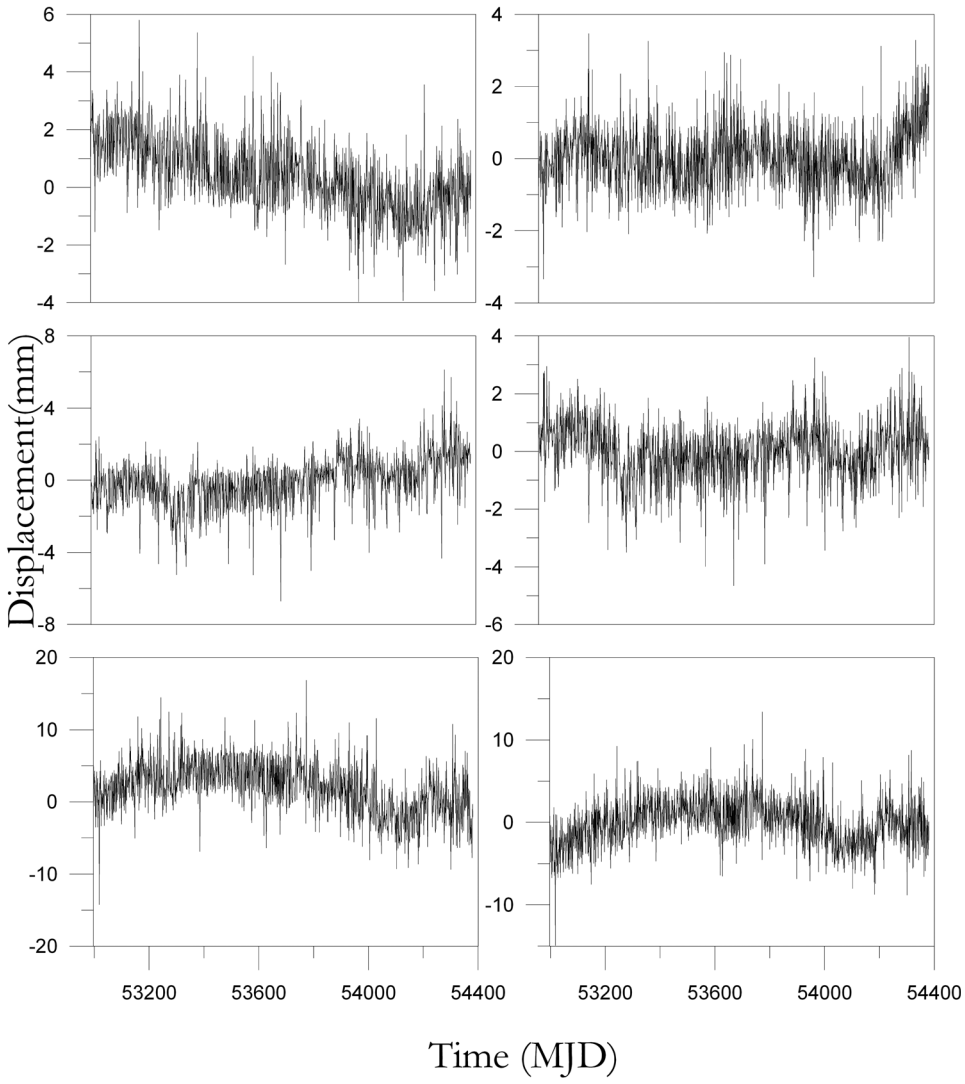

Figure 3. Example of GPS time series, recorded at the ENAV station, (left) before and (right) after filtering: (top) north, (middle) east, and (bottom) up components. MJD, modified Julian date.

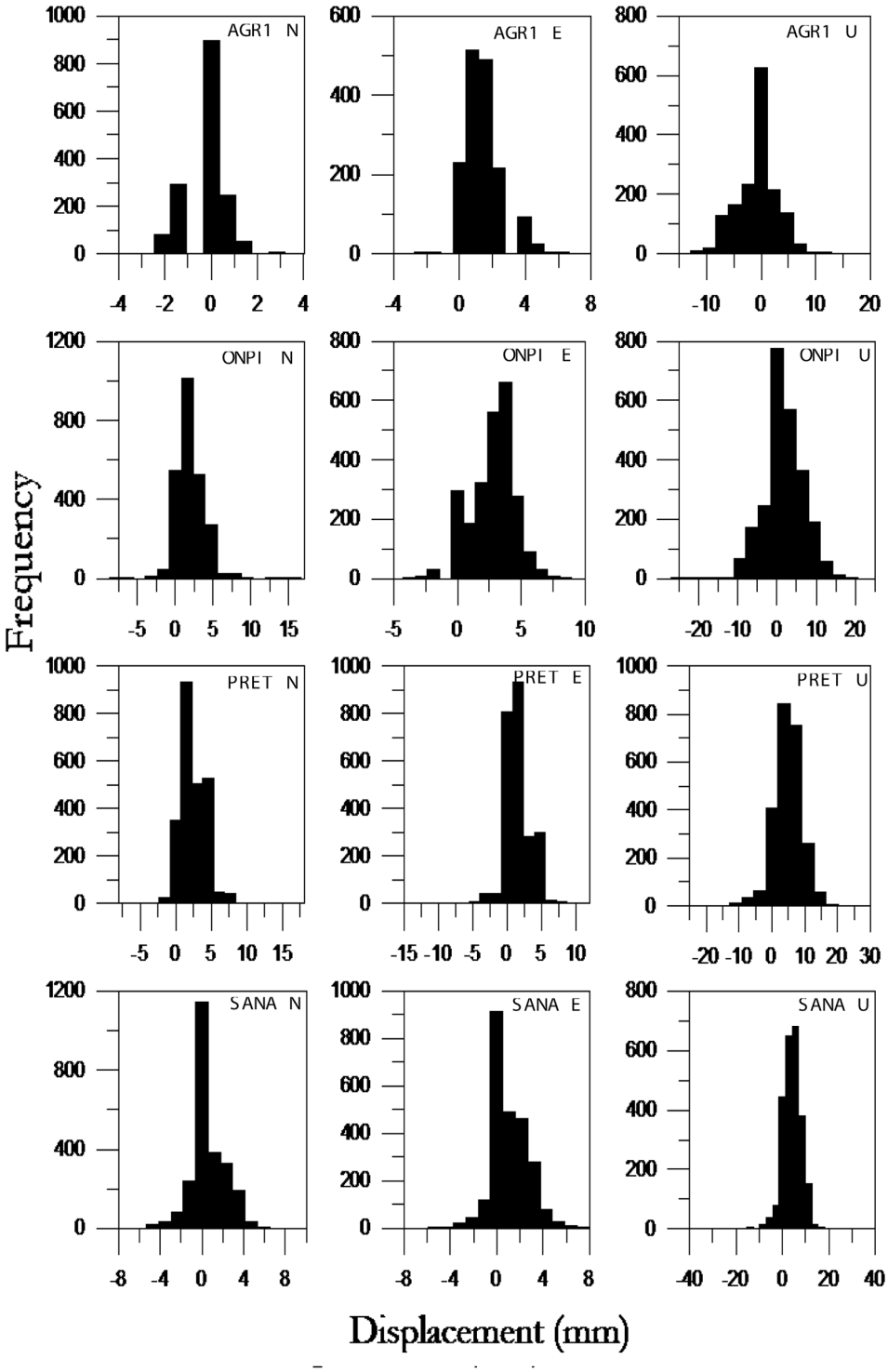

Figure 4. Distribution of the ground deformation: relative stations and components (N, north–south; E, east–west, U, up) are reported.

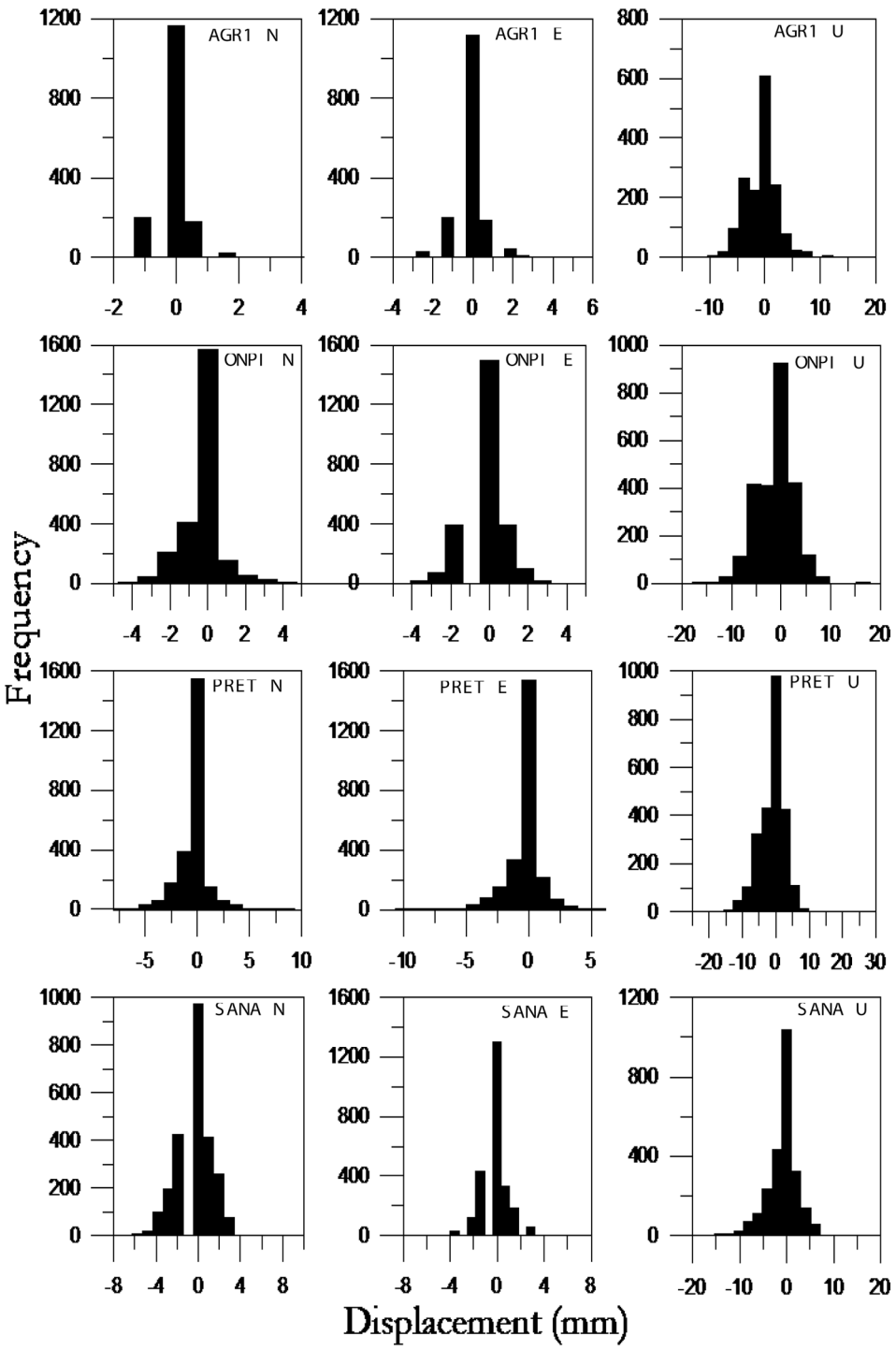

Figure 5. Distribution of the filtered signals: relative stations and components (N, north–south; E, east–west; U, up) are reported.

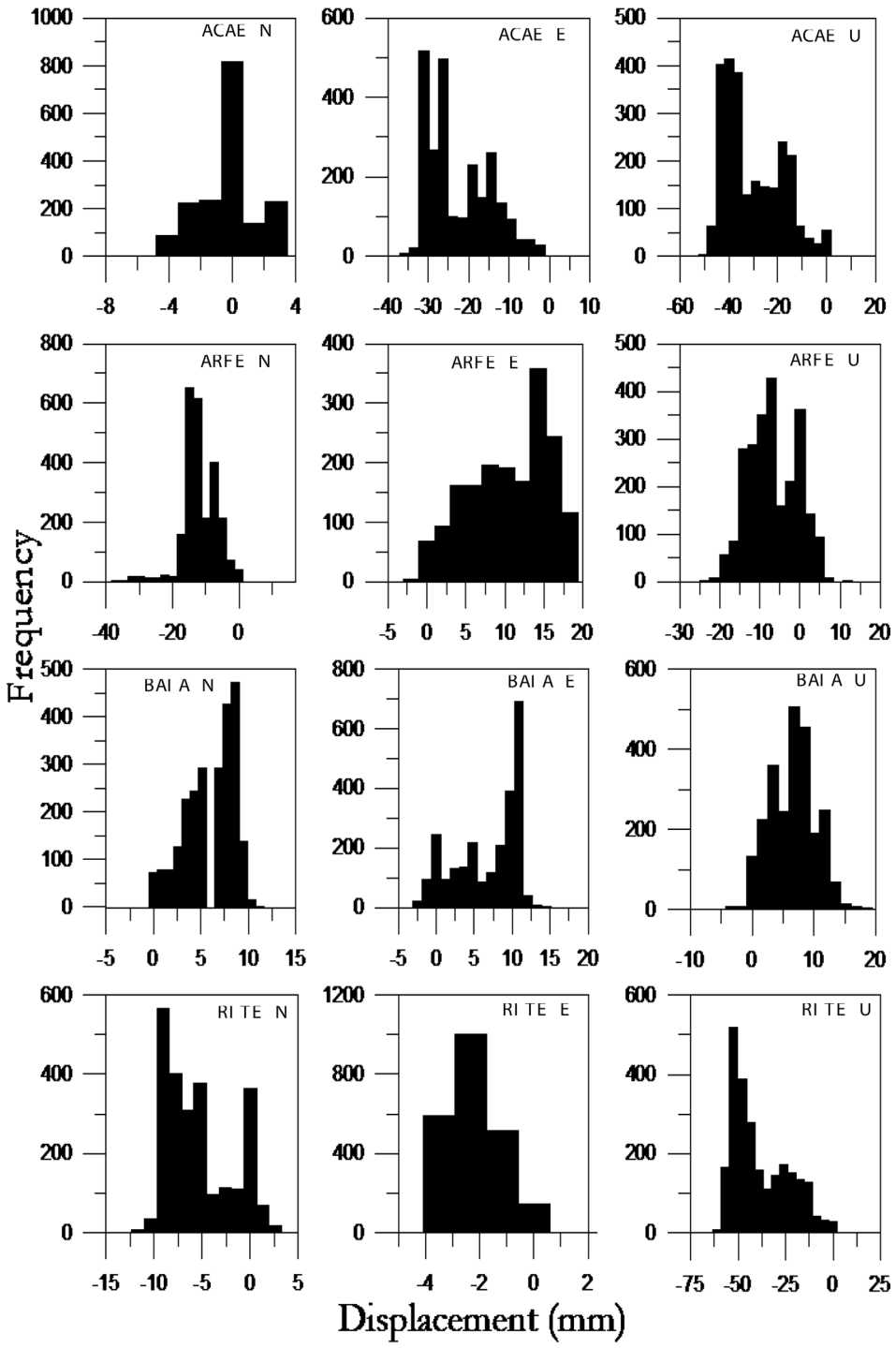

Figure 6. Distribution of the ground deformation: relative stations and components (N, north–south; E, east–west; U, up) are reported.

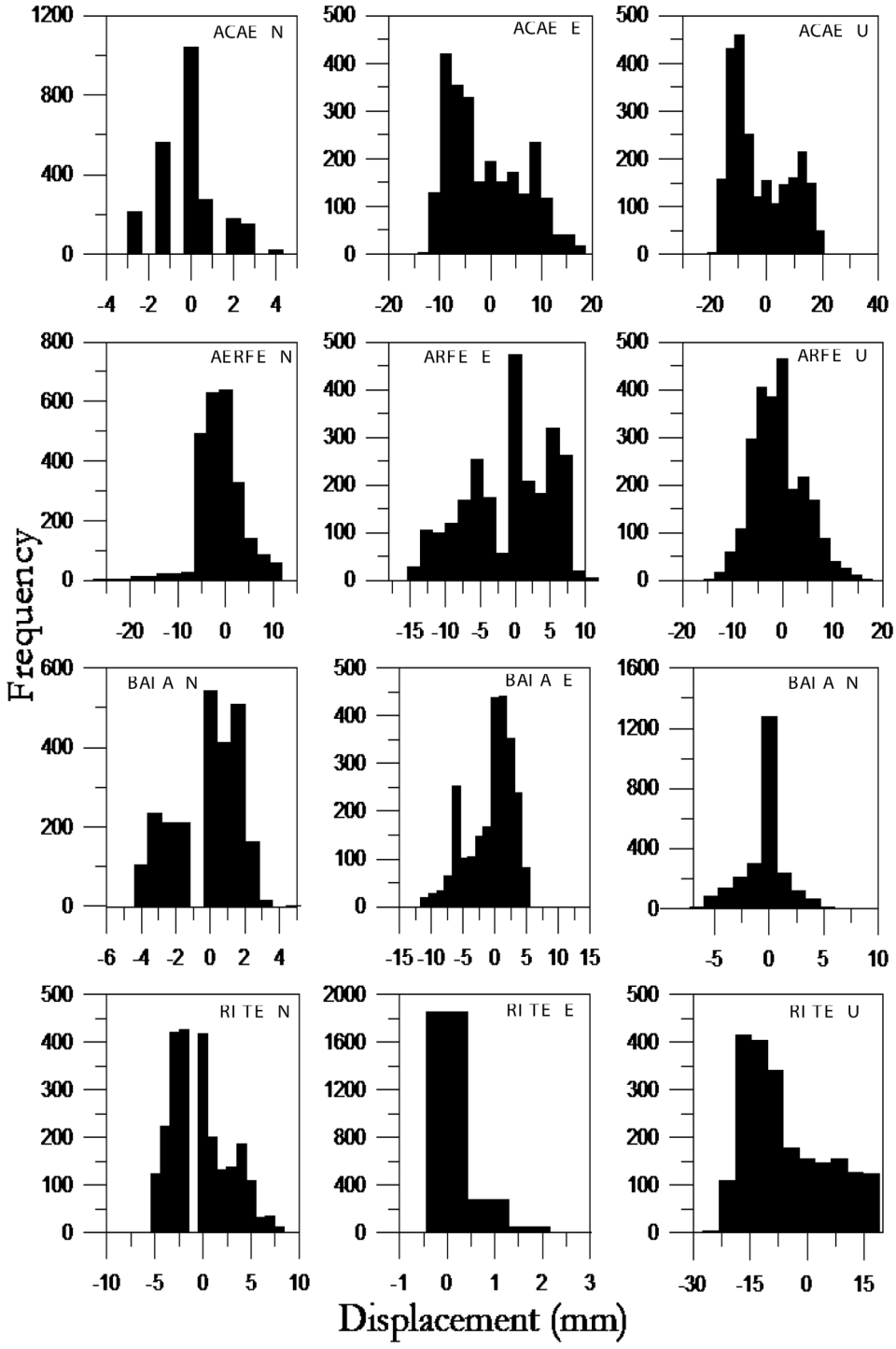

Figure 7. Distribution of the filtered signals: relative stations and components (N, north–south; E, east–west; U, up) are reported.

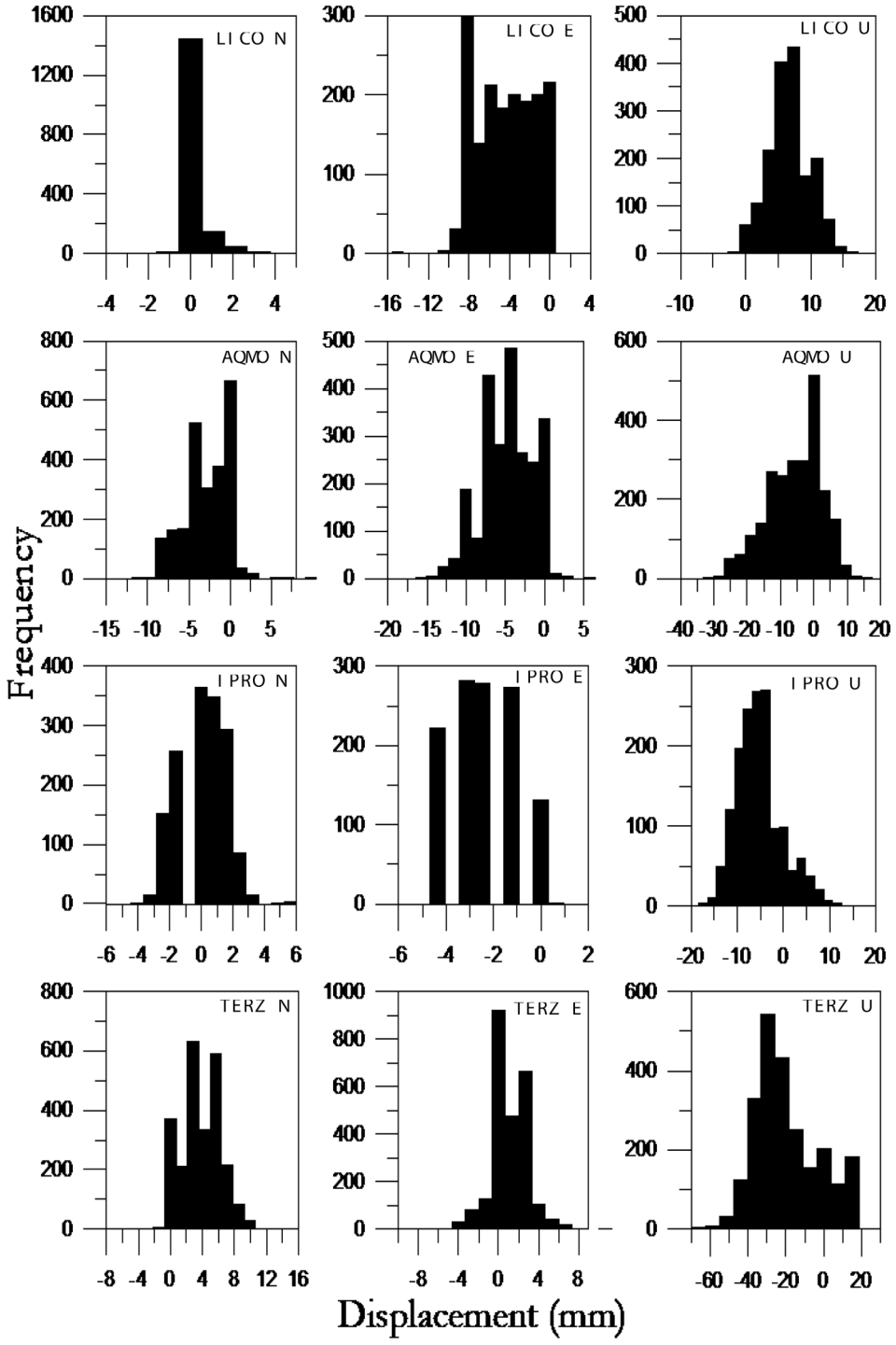

Figure 8. Distribution of the ground deformation: relative stations and components (N, north–south; E, east–west; U, up) are reported.

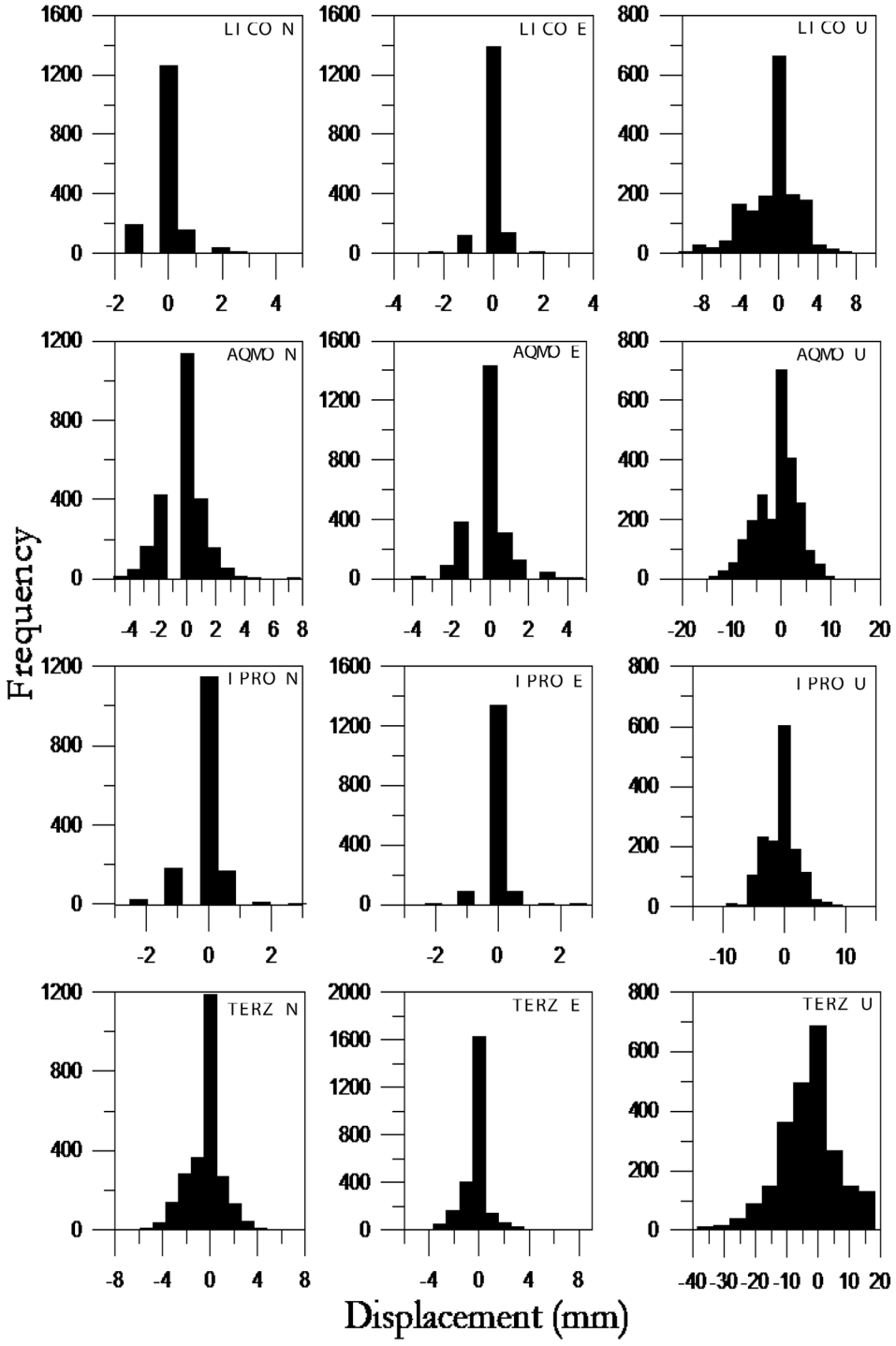

Figure 9. Distribution of the filtered signals: relative stations and components (N, north–south; E, east–west; U, up) are reported.

Table 1. Values of κ for All Analyzed Stations[a]

Station	North	East	Up	Station	North	East	Up
ACAE	−0.78	−0.76	−0.64	LICO	25.47	−0.85	0.52
	−0.29	−0.98	−0.97		4.29	1.76	0.17
AGR1	0.43	1.60	0.63	MORU	−0.01	0.05	0.09
	0.64	1.13	1.41		−0.23	−0.58	0.55
AQMO	0.35	−0.34	−0.44	ONPI	2.90	0.20	0.55
	1.06	0.92	0.01		1.78	0.93	1.09
ARFE	3.24	−0.86	−0.66	PRET	3.68	2.13	2.55
	2.15	−1.03	−0.52		2.13	1.10	1.30
BAIA	−0.29	−0.73	−0.14	QUAR	−0.02	−0.61	0.24
	−0.83	−0.64	0.78		−0.80	−0.06	−0.29
ENAV	0.21	1.54	0.35	RITE	−0.63	0.57	−0.68
	0.61	1.01	0.69		−0.54	0.17	−0.72
IPPO	−0.30	−0.59	−0.67	SANA	−0.13	0.49	1.23
	−0.15	−0.75	−0.46		−0.12	0.32	0.78
IPRO	−0.82	−0.80	0.54	TERZ	−0.53	0.61	−0.41
	1.21	2.72	0.78		−0.43	0.93	0.49

[a]First row for each station, before filtering; second row, after filtering.

ground deformation, which was attributed to a pressure source located approximately beneath Pozzuoli [*Troise et al.*, 2007, 2008]. Very similar results were also obtained by tide gauge [*Tammaro et al.*, 2007], leveling data [*Pingue et al.*, 2006; *Troise et al.*, 2008], and SAR [*Trasatti et al.*, 2008] observations. The deformation field is in very good agreement with the bimodal amplitude distribution.

4. Fit and Simulation of Ground Deformation

[23] To model the time evolution of the ground deformation, we fitted the time series at each station with polynomials of different order by means of a standard chi-square minimization procedure. As an example, the vertical ground deformation at the RITE station is shown in Figure 11a, where it is possible to observe polynomial fits up to eight orders. A standard analysis of the variance (F test) reveals, within a 95% confidence level, that we obtain the best fit with a fifth-order polynomial.

[24] The same order of polynomial fits the time series recorded at the other stations very well, but obviously with different values of the coefficients. In Figures 11b and 11c, we show representative examples of how the polynomial fits different components at stations located in the investigated area. Specifically, the case of Baia is reported in Figure 11b as another example in Campi Flegrei; instead the Vesuvian area ground deformation fit is illustrated in Figure 11c by the station AGR1. Therefore, we can reasonably assume this fit as the model of the deformation history in the area.

[25] A further indication that this polynomial well represents the deformation history can be obtained by simply subtracting the fit from the signal. If the residual signal distribution is more similar to that of the signals not affected by deformation, we can accept the hypothesis. In Figure 12 we show the original and residual time series at the RITE station and their distributions for the vertical component. It is clear that the residual signal exhibits a more peaked distribution and that the second mode disappears; indeed, κ changes from −0.68 to 0.11 when we subtract the polynomial. A very similar result is obtained for the other stations with κ values in the range 0.91–2.14 for the residual signals. This is a clear indication that the fitted polynomial represents the deformation history.

[26] As a counterproof, we subtracted the fitted fifth-order polynomial from signals that do not exhibit any observable ground deformation. Figure 13 shows an example of the original and residual signals with their amplitude distributions for the ENAV vertical component. As can be seen in this case, the distribution becomes more broad for the residual signal; indeed, κ changes from 0.35 to −1.18.

[27] Finally, we performed a very simple simulation of the deformation time evolution to qualitatively identify when the Gaussian amplitude distribution of the background is modified by ground movements. Namely, we generated a Laplacian noise (super-Gaussian) with zero mean and a standard deviation of the same order of magnitude of the fifth-order polynomial amplitude. Then we overlapped this time series and two signals which should represent typical ground deformation histories: a hyperbolic tangent and a Gaussian impulse. The first one is a representation of a

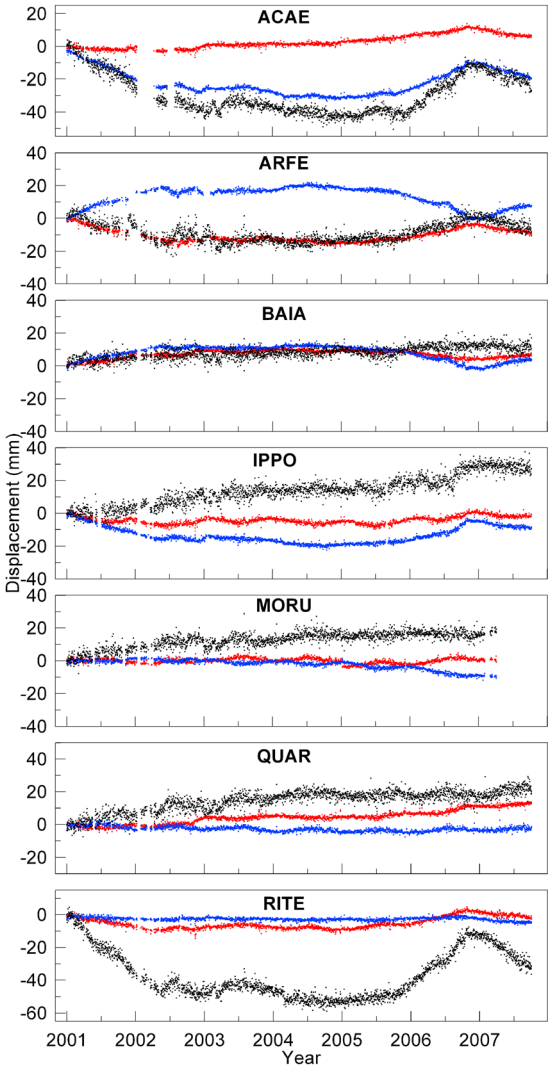

Figure 10. GPS time series recorded at the Campi Flegrei stations (red, north–south component; blue, east–west component; black, vertical component) where we observe a sub-Gaussian amplitude distribution for at least one component (see Table 1).

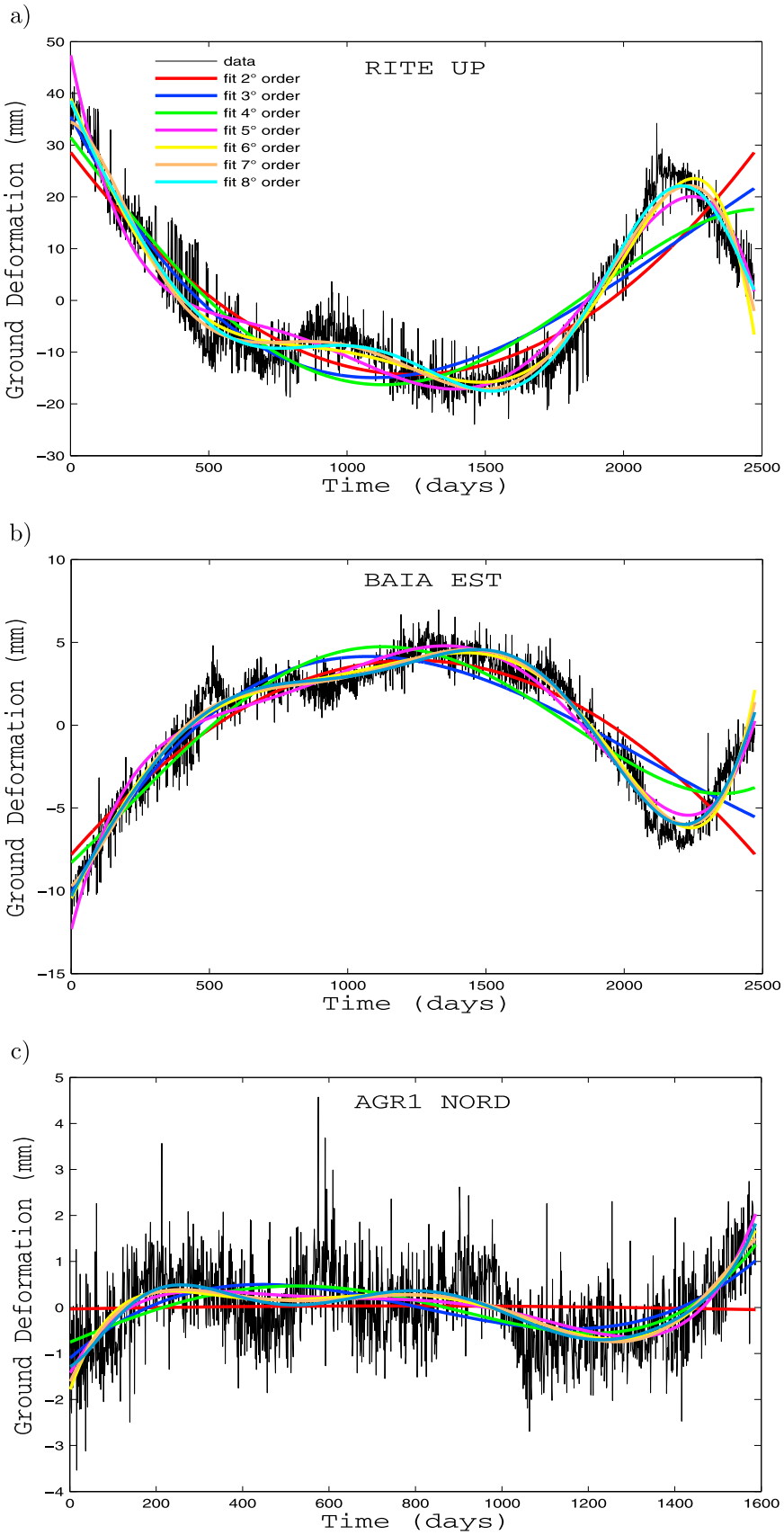

Figure 11. GPS time series recorded at different stations and components. Continuous colored curves are the fits.

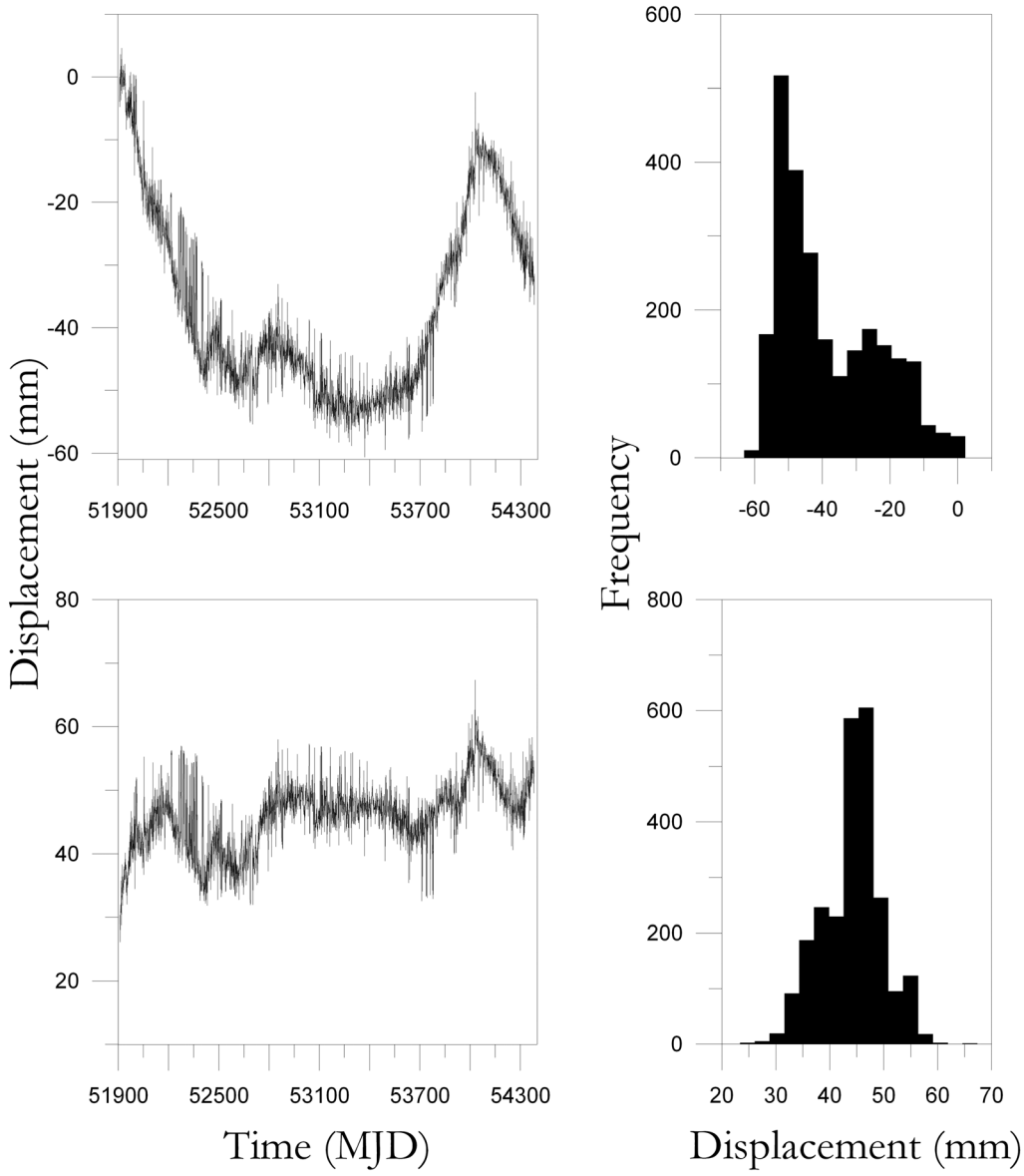

Figure 12. (left) Vertical component of the (top) original and (bottom) residual signals at the RITE station with their (right) amplitude distributions.

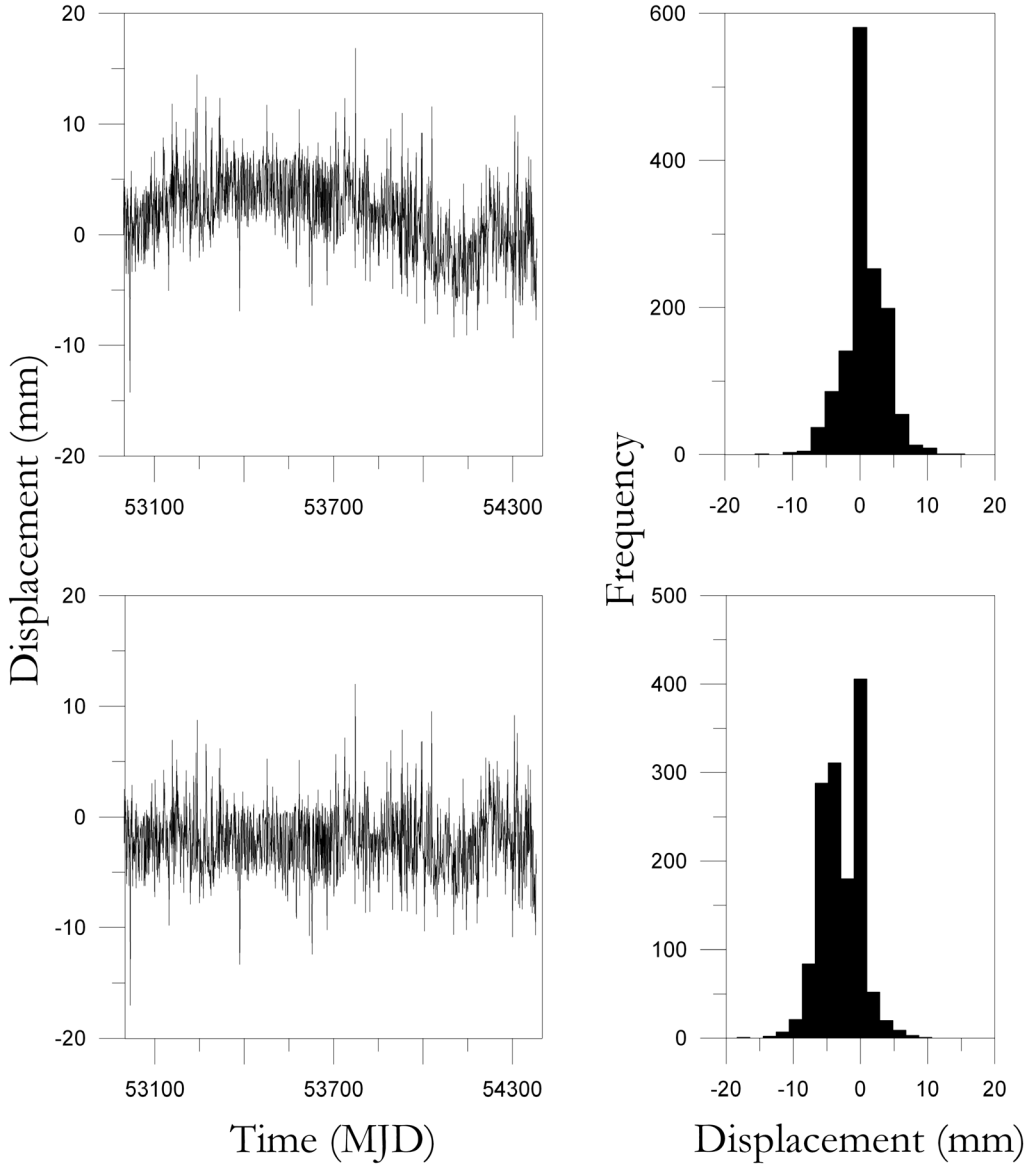

Figure 13. (left) Vertical component of the (top) original and (bottom) residual signals at the ENAV station with their (right) amplitude distributions.

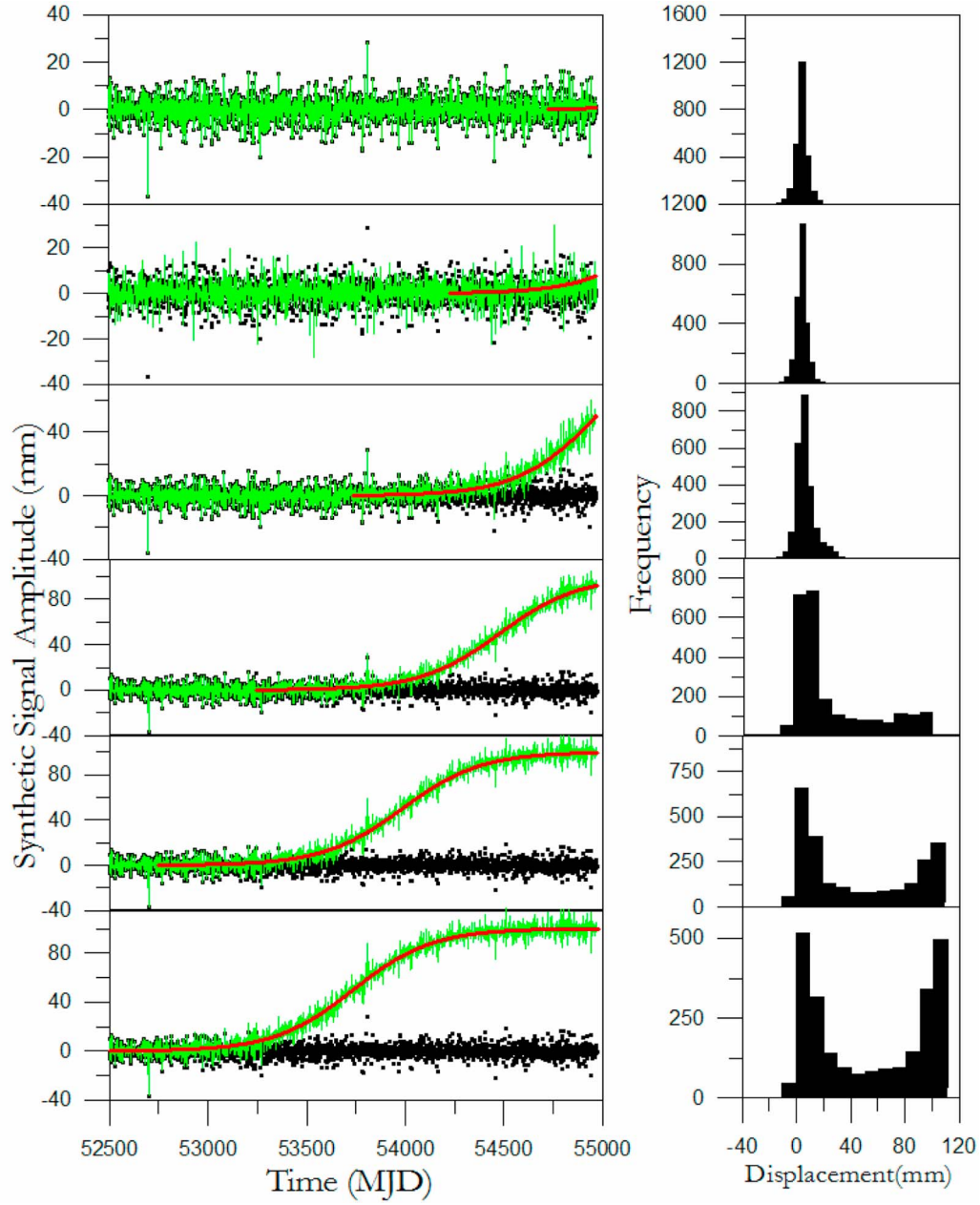

Figure 14. (left) Simulated time series (black circles, Laplace noise; red line, hyperbolic tangent; green line, their superposition) and (right) amplitude distributions for the different overlapping windows: $D/10$, $3D/10$, $D/2$, $7D/10$, $9D/10$, and D from top to bottom. Here we report the signal with $A = 50$ mm.

ground deformation evolving continuously from a zero deformation level to a given permanent deformation. The second one is a representation of a scenario in which the ground is deformed to a certain level and then returns to a zero deformation level. The superposition of the Laplacian noise and of the two signals, representing the deformation history, was performed for different time windows ($D/10$, $D/5$, $3D/10$, $2D/5$, $D/2$, $3D/5$, $7D/10$, $4D/5$, $9D/10$, and D, where D is the total duration of the Laplacian noise time series) and different amplitude of the displacement ($A = 25$, 50, and 75 mm). Thereby we constructed new signals whose first part is the Laplacian noise and the last is the superposition of noise and simulated ground deformation within the overlapping window T. Then we analyzed the amplitude distributions of these new series. An example for $A = 50$ mm is illustrated in Figures 14 and 15 for the hyperbolic tangent and Gaussian impulse, respectively. A qualitative inspection of the amplitude distributions (Figures 14 and 15, right) reveals that, as T increases, the distribution becomes broader and a second mode clearly appears at larger values of the ground deformation when $T = D/2$. Notice that we observe a non-Gaussian distribution with a kurtosis approximately equal to zero depending on the relative amplitudes of the background noise and impulse.

[28] A more quantitative evaluation of the distribution evolution can be obtained by means of κ (Figures 16 and 17);

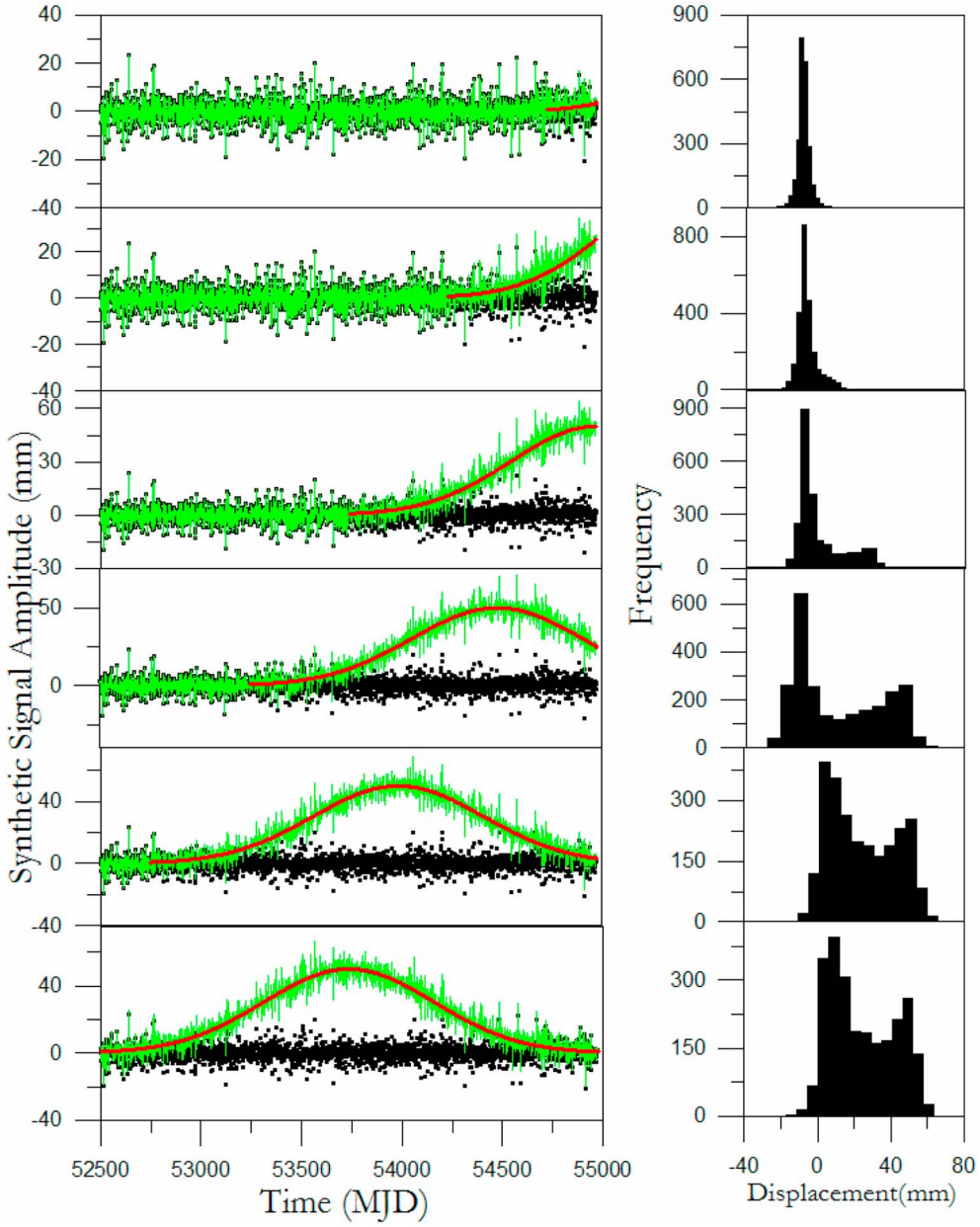

Figure 15. (left) Simulated time series (black circles, Laplace noise; red line, Gaussian impulse; green line, their superposition) and (right) amplitude distributions for the different overlapping windows: $D/10$, $3D/10$, $D/2$, $7D/10$, $9D/10$, and D from top to bottom. Here we report the signal with $A = 50$ mm.

indeed, it decreases approximately linearly with T for both synthetic displacement histories. Notice that using the Gaussian impulse κ reaches a stable value for $T > 3D/5$. This behavior appears to be independent of the displacement amplitude. The rapid appearance of a second mode in the distributions can be easily interpreted by observing that the noise amplitude is modulated by the ground deformation.

5. Conclusions

[29] We analyzed the amplitude distribution of 16 GPS time series recorded at the NeVoCGPS network for the Neapolitan volcanic area. The distributions exhibit a super-Gaussian behavior, although when we observe a clear ground deformation, they become bimodal. The analysis of the kurtosis more quantitatively confirmed this observation. This peculiar feature was identified as a marker of the occurrence of a significant deformation. Ground movements were modeled using a fifth-order polynomial representing its time evolution. When we remove the model from the recorded signal, we recover a super-Gaussian amplitude distribution for the residual time series. This is a clear indication that the polynomial represents a good fit of the deformative history. Moreover, a simulation of the time evolution of the deformation indicates that κ decreases monotonically as the ground deformation increases in time. The extension of our

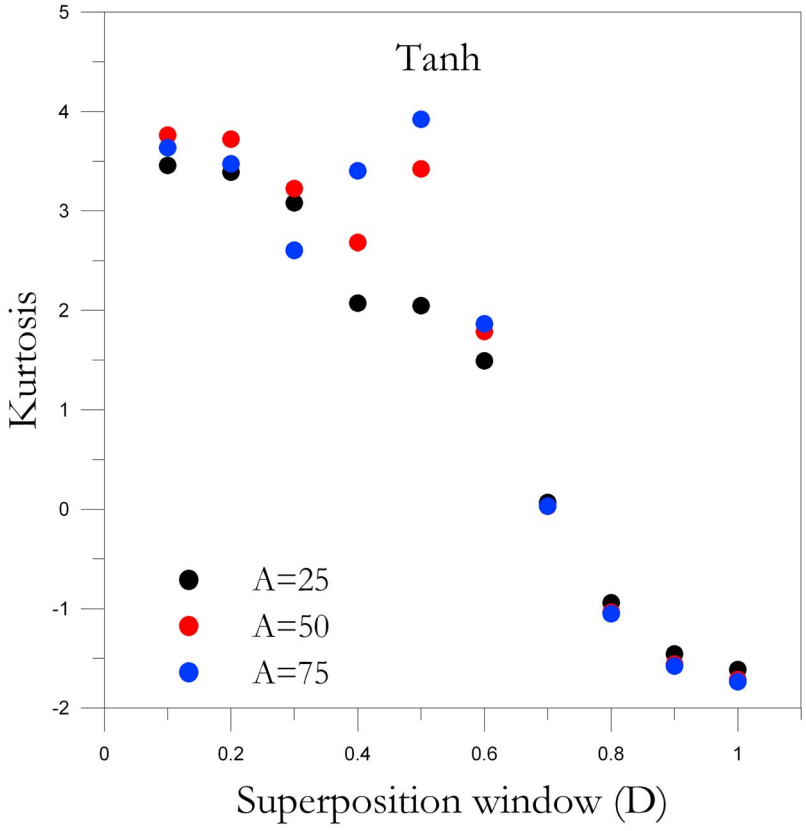

Figure 16. Estimated kurtosis for the hyperbolic tangent as a function of T for different values of A.

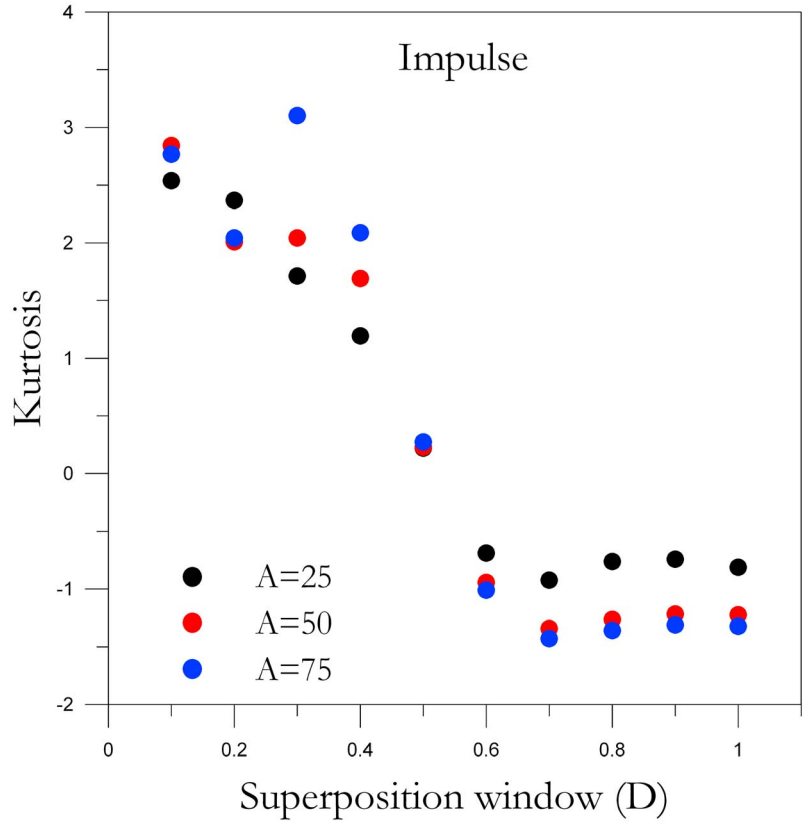

Figure 17. Estimated kurtosis for a Gaussian impulse as a function of T for different values of A.

results to other volcanic areas in the world and the analysis of longer time series could be very interesting for volcano monitoring.

[30] The presented approach represents a contribution aimed at adding further information to the studies about the deformation in the Neapolitan volcanic area by revealing geologically relevant data. Moreover, the results suggest that the continuous monitoring of the GPS data properties in this area could be useful to detect the insurgence of the background deformation level. This task is of fundamental importance in densely populated high-risk volcanic areas such as Campi Flegrei-Vesuvio.

[31] **Acknowledgments.** This research was partially supported by the 2004–2006 INGV-DPC Project in Volcanology and by 2001–2009 DPC-INGV contracts.

References

Battaglia, M., C. Troise, F. Obrizzo, F. Pingue, and G. De Natale (2006), Evidence for fluid migration as the source of deformation at Campi Flegrei caldera (Italy), *Geophys. Res. Lett.*, *33*, L01307, doi:10.1029/2005GL024904.

Bell, A. J., and T. J. Sejnowski (1995), An information-maximisation approach to blind separation and blind deconvolution, *Neur. Comput.*, *7*, 1129–1159.

Beran, J. (1994), *Statistic for Long-Memory Processes*, *Monogr. on Stat. and Appl. Probab.*, vol. 61, 315 pp., Chapman and Hall, New York.

Bottiglieri, M., M. Falanga, U. Tammaro, F. Obrizzo, P. De Martino, C. Godano, and F. Pingue (2007), Independent component analysis as a tool for ground deformation analysis, *Geophys. J. Int.*, *168*, 1305–1310.

Carlino, S., E. Cubellis, G. Luongo, and F. Obrizzo (2006), On the mechanics of caldera resurgence of Ischia Island (southern Italy), in *Mechanisms of Activity and Unrest at Large Calderas*, vol. 269, edited by C. Troise, G. De Natale, and C. R. J. Kilburn, pp. 181–193, Geol. Soc., London.

Dach, R., U. Hugentobler, P. Fridez, and M. Meindl (2007), *User Manual of the Bernese GPS Software 5.0*, Astron. Inst., Univ. of Bern, Bern, Switzerland.

De Martino, P., U. Tammaro, G. Brandi, A. D'Alessandro, M. Dolce, T. Esposito, S. Malaspina, F. Obrizzo, F. Pingue, and C. Serio (2007), Area vulcanica Napoletana: 10 anni di ossservazioni GPS, in *Proceedings of the 11th ASITA National Conference* (in Italian), vol. I, pp. 925–930.

De Natale, G., C. Troise, F. Pingue, P. De Gori, and C. Chiarabba (2001), Structure and dynamics of the Somma-Vesuvius volcanic complex, *Mineral. Petrol.*, *73*(1–3), 5–22.

De Natale, G., C. Troise, F. Pingue, G. Mastrolorenzo, and L. Pappalardo (2006), The Somma-Vesuvius volcano (Southern Italy): Structure, dynamics and hazard evaluation, *Earth. Sci. Rev.*, *74*, 73–111.

Dong, D., P. Fang, Y. Bock, M. K. Cheng, and S. Myazaki (2002), Anatomy of apparent seasonal variations from GPS-derived site position time series, *J. Geophys. Res.*, *107*(B4), 2075, doi:10.1029/2001JB000573.

Dow, J. M., R. E. Neilan, and C. Rizos (2009), The International GNSS Service in a changing landscape of Global Navigation Satellite Systems, *J. Geodesy*, *83*, 191–198, doi:10.1007/s00190-008-0300-3.

Ferland, R. (2006), Proposed update of the IGS reference frame realization, paper presented at IGS Workshop, Darmstadt, Germany.

Gaeta, F. S., F. Peluso, I. Arienzo, D. Castagnolo, G. De Natale, G. Milano, C. Albanese, and D. G. Mita (2003), A physical appraisal of a new aspect of bradyseism: The miniuplifts, *J. Geophys. Res.*, *108*(B8), 2363, doi:10.1029/2002JB001913.

Hyvärinen, A., J. Karhunen, and E. Oja (2001), *Independent Component Analysis*, John Wiley, New York.

Judenherc, A., and A. Zollo (2004), The Bay of Naples (southern Italy): Constraints on the volcanic structures inferred from dense seismic survey, *J. Geophys. Res.*, *109*, B10312, doi:10.1029/2003JB002876.

Karhunen, J. (1996), Neural approach to independent component analysis and sources separation, in *Proceedings of Fourth European Symposium on Artificial Neural Networks*, pp. 249–266.

Langbein, J., and H. Johnson (1997), Correlated errors in geodetic time series: Implications for time-dependent deformation, *J. Geophys. Res.*, *102*(B1), 591–603.

Mangiarotti, S., A. Cazenave, L. Soudarin, and J. F. Crétaux (2001), Annual vertical crustal motions predicted from surface mass redistribution and observed by space geodesy, *J. Geophys. Res.*, *106*(B3), 4277–4291.

Mao, A., C. G. A. Harrison, and T. H. Dixon (1999), Noise in GPS coordinate time series, *J. Geophys. Res.*, *104*(B2), 2797–2816, doi:10.1029/1998JB900033.

Patacca, E., and P. Scandone (2007), Geology of the Southern Apennines, *Boll. Soc. Geol. Ital.*, *7*, 75–119.

Pingue, F., P. De Martino, F. Obrizzo, C. Serio, and U. Tammaro (2006), Stima del campo di spostamento ai Campi Flegrei da dati GPS e di livellazione di precisione nel periodo Maggio 2004–Marzo 2006 (in Italian), *Open File Rep. 5*, Vesuvius Obs., Natl. Inst. of Geophys. and Volcanol., Naples, Italy.

Ray, J., D. Dong, and Z. Altamimi (2004), IGS reference frames: Status and future improvements, *GPS Solutions*, *8*(4), 251–266, doi:10.1007/s10291-004-0110-x.

Scandone, P. (1979), Origin of the Thyrrenian Sea arc, *Boll. Soc. Geol. Ital.*, *98*, 27–34.

Schmid, R., P. Steigenberger, G. Gendt, M. Ge, and M. Rothacher (2007), Generation of a consistent absolute phase center correction model for GPS receiver and satellite antennas, *J. Geodesy*, *81*(12), 781–798, doi:10.1007/s00190-007-0148-y.

Steigenberger, P., M. Rothacher, R. Dietrich, M. Fritsche, A. Rülke, and S. Vey (2006), Reprocessing of a global GPS network, *J. Geophys. Res.*, *111*, B05402, doi:10.1029/2005JB003747.

Tammaro, U., F. Di Sena, P. Capuano, F. Obrizzo, A. La Rocca, S. Pinto, A. Russo, P. De Martino, and F. Pingue (2007), Deformazioni del suolo mediante analisi dei dati mareografici nell'area vulcanica napoletana nel periodo 1999–2006, in *Proceedings of the 11th ASITA National Conference* (in Italian), vol. II, pp. 2079–2084.

Trasatti, E., et al. (2008), The 2004–2006 uplift episode at Campi Flegrei caldera (Italy): Constraints from SBAS-DInSAR ENVISAT data and Bayesian source inference, *Geophys. Res. Lett.*, *35*, L07308, doi:10.1029/2007GL033091.

Troise, C., G. De Natale, F. Pingue, F. Obrizzo, P. De Martino, U. Tammaro, and E. Boschi (2007), Renewed ground uplift at Campi Flegrei caldera (Italy): New insight on magmatic processes and forecast, *Geophys. Res. Lett.*, *34*, L03301, doi:10.1029/2006GL028545.

Troise, C., G. De Natale, F. Pingue, U. Tammaro, P. De Martino, F. Obrizzo, and E. Boschi (2008), A new uplift episode at Campi Flegrei caldera (southern Italy): Implications for unrest interpretation and eruption hazard evaluation, *Dev. Volcanol.*, *10*, 375–392, doi:10.1016/S1871-644X(07)00010-1.

van Dam, T., G. Blewitt, and M. Heflin (1994), Atmospheric pressure loading effects on Global Positioning System coordinate determinitions, *J. Geophys. Res.*, *99*(B12), 23,939–23,950, doi:10.1029/94JB02122.

Watson, C., P. Tregoning, and R. Coleman (2006), Impact of solid Earth tide models on GPS coordinate and tropospheric time series, *Geophys. Res. Lett.*, *33*, L08306, doi:10.1029/2005GL025538.

Williams, S. D. P. (2003), The effect of colored noise on the uncertainties of rates estimated from geodetic time series, *J. Geodesy*, *76*, 483–494.

Williams, S. D. P., Y. Bock, P. Fang, P. Jamason, R. M. Nikolaidis, L. Prawirodirdjo, M. Miller, and M. Johnson (2004), Error analysis of continuous GPS time series, *J. Geophys. Res.*, *109*, B03412, doi:10.1029/2003JB002741.

M. Bottiglieri and C. Godano, Dipartimento di Scienze Ambientali, Seconda Università degli Studi di Napoli, via Vivaldi 43, I-81100 Caserta, Italy. (milena.bottiglieri@unina2.it; cataldo.godano@unina2.it)

P. De Martino, F. Obrizzo, F. Pingue, and U. Tammaro, Istituto Nazionale di Geofisica e Vulcanologia, Osservatorio Vesuviano, via Diocleziano 328, I-80124 Naples, Italy.

M. Falanga, Dipartimento di Matematica e Informatica, Università di Salerno, via Ponte Don Melillo, I-84084 Fisciano (SA), Italy.